SPHERIODIZATION OF THE GRAIN BOUNDARY PRECIPITATES
IN Fe-Ta-Cr ALLOYS

INDEX

		Page
ABSTRACT		v
I.	INTRODUCTION	1
II.	EXPERIMENTAL PROCEDURE	5
	A. Alloy Preparation	5
	B. Dilatometer Analysis	5
	C. Heat Treatments	5
	D. Hardness Tests	14
	E. Tensile Tests	14
	F. X-ray Analysis of the Second Phase Particles	16
	G. Optical Microscopy	16
	H. Scanning Electron Microscopy	16
III.	RESULTS AND DISCUSSIONS	18
	A. Phase Relations in the Fe-Ta-Cr Ternary System	18
	B. Morphology and Kinetics of Laves Phase Precipitation	20
	C. Spheroidization of Grain Boundary and Matrix Precipitates	23
	D. Mechanical Properties	27
IV.	CONCLUSIONS	45
ACKNOWLEDGMENTS		46
REFERENCES		47
FIGURE CAPTIONS		48

SPHEROIDIZATION OF THE GRAIN BOUNDARY PRECIPITATES IN Fe-Ta-Cr ALLOYS

Sungho Jin

Inorganic Materials Research Division, Lawrence Berkeley Laboratory
and Department of Materials Science and Engineering,
College of Engineering; University of California,
Berkeley, California 94720

ABSTRACT

The partly continuous grain boundary precipitates were fully spheroidized by cycling through the α-γ phase transformation. Both the ductility and strength were increased by the spheroidization treatment. The effect of chromium on the Fe-Ta binary system was found to enhance spheroidization as well as improve oxidation resistance.

I. INTRODUCTION

Recently several binary systems of Fe-Ta, Fe-Nb, Fe-Ti, Fe-Zr, and Fe-Hf have been studied with the objective of developing carbon-free age hardenable iron base alloys. Such alloys contain a fine dispersion of Laves phase precipitates (Fe_2Ta, Fe_2Nb, Fe_2Ti, Fe_2Zr, and Fe_2Hf) but also have grain boundary films of the second phase. The highest strength Laves phase alloys were found to be those containing Fe_2Nb and Fe_2Ta.[1] In Russel H. Jones' recent work,[2] the brittle fracture characteristic of Fe-Ta alloy was eliminated by the use of simple $\alpha \rightarrow \gamma$ transformation which spheroidized the continuous grain boundary network. However, the relatively high solution treating temperature required caused oxidation of the alloy, and coarsening of precipitate particles during the spheroidization treatment occurred.

Previous studies on Laves phase alloys have been confined to binary alloys. The ternary phase diagram of Fe-Ta-Cr system, which would have been helpful in the present work, has not been reported in the literature. The binary phase diagrams are shown in Figs. 1, 2, and 3.

The objective of this investigation was to determine the effect of chromium addition on the properties of Fe-Ta alloy. This involved the determination of the approximate phase diagram, study on the aging characteristics, measurement of mechanical properties and the determination of the heat treatment required for grain boundary spheroidization.

From the practical point of view, one objective of this study was to provide a basis for developing improved high temperature creep resisting alloys.

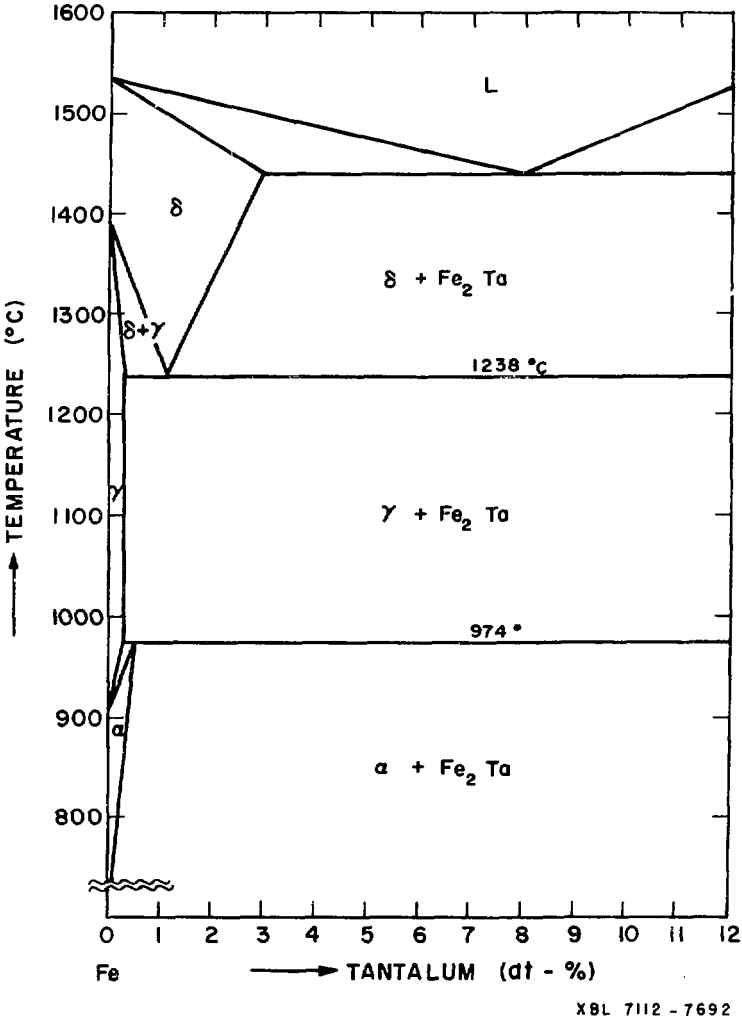
1600
1500
1400
1300
1200
1100
1000
900
800
TEMPERATURE (°C)
L
δ
δ + Fe2 Ta
δ+γ
1238 °C
γ
γ + Fe2 Ta
974 °
α
α + Fe2 Ta
0 1 2 3 4 5 6 7 8 9 10 11 12
Fe
TANTALUM (at - %)
XBL 7112 - 7692

Fig. 1

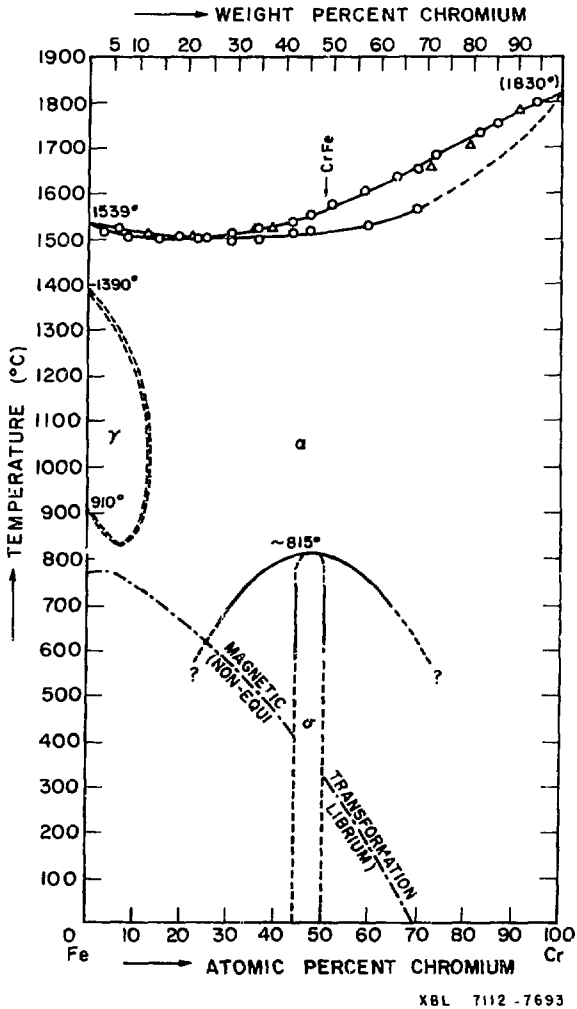
WEIGHT PERCENT CHROMIUM
5 10 20 30 40 50 60 70 80 90
1900
1800
1700
1600
1500
1400
1300
1200
1100
1000
900
800
700
600
500
400
300
200
100
0
(1830°)
CrFe
1539°
1390°
γ
α
910°
~815°
?
MAGNETIC
NON-EQUI
δ
?
TRANSFORMATION
LIBRIUM
TEMPERATURE (°C)
10 20 30 40 50 60 70 80 90 100
Fe
Cr
ATOMIC PERCENT CHROMIUM
XBL 7112-7693

Fig. 2

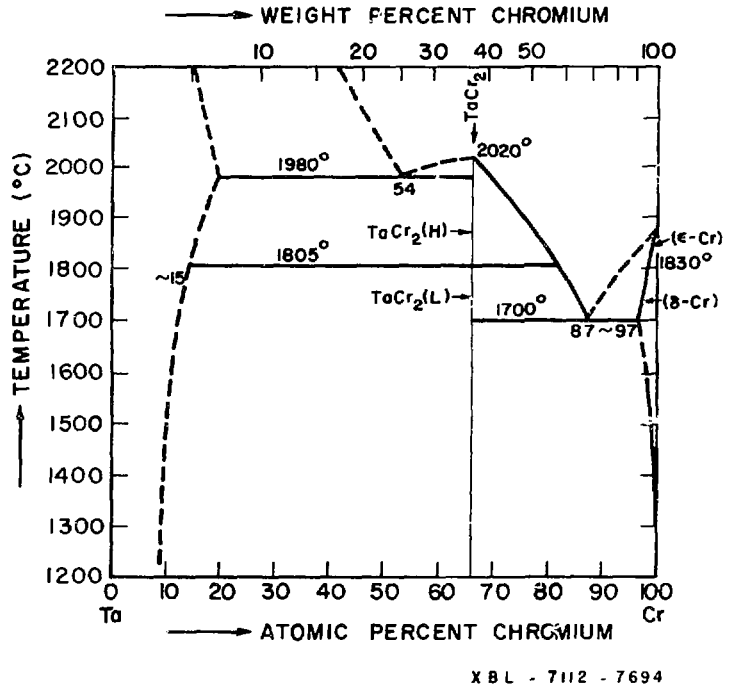
WEIGHT PERCENT CHROMIUM
10
20
30
40
50
100
2200
2100
2000
1900
1800
1700
1600
1500
1400
1300
1200
TEMPERATURE (°C)
TaCr2
1980°
2020°
54
TaCr2(H)
1805°
~15
TaCr2(L)
1700°
87~97
(ε-Cr)
1830°
(β-Cr)
0
10
20
30
40
50
60
70
80
90
100
Ta
Cr
ATOMIC PERCENT CHROMIUM
XBL - 7112 - 7694

Fig. 3

II. EXPERIMENTAL PROCEDURE

A. Alloy Preparation

Six Fe-Ta-Cr alloys of different composition were prepared from 99.95% purity electrolytic iron, 99.9% three pass zone refined tantalum rod of 0.3" diameter and 99.9% chromium. A vacuum induction furnace was used for the melting; the melt was held at 1750°C for 30 minutes in an MgO crucible under an argon atmosphere.

One and one-quarter inch diameter ingots were cast and hot rolled at 1000°C into 1/2" square rods. The compositions of the six alloys are shown in Table I.

B. Dilatometer Analysis

To determine the α-γ and γ-δ phase transformation temperatures of each alloy, a differential dilatometer was used. Bars of 0.25" diameter and 2.5" length were used. The method employed is shown schematically in Fig. 4. Differential expansion of the bar during heating was converted into electrical signal which was amplified and recorded. The specimens were heated at a rate of 10°C/minute and argon gas was passed continuously over the specimen to reduce oxidation and scaling. Above 1200°C, the SiO_2 bar started to bend and the accuracy was therefore limited at the higher temperatures. The results of this dilatometer analysis are shown in Table II.

C. Heat Treatments

All specimens were encapsulated in quartz tubes (0.3 atmospheric pressure of argon gas at room temperature) and solution treated at 1320°C for 1 hour. The specimens were quenched into iced 10% salt water (Fig. 5-Fig. 9). Specimens for α-γ phase transformation temperature

TABLE I. COMPOSITIONS AND HEAT TREATMENTS OF THE DESIGNED ALLOYS

	Ta	Cr	Fe	Solution Treatment	Aging
Fe 1 Ta 3Cr	1%	3%	Balanced	1320°C, 1 hour	700°C, 40 minutes
Fe 1 Ta 5Cr	1%	5%	Balanced	1320°C, 1 hour	700°C, 40 minutes
Fe 1 Ta 7Cr	1%	7%	Balanced	1320°C, 1 hour	700°C, 40 minutes
Fe 2 Ta 3Cr	2%	3%	Balanced	1370°C, 1 hour	700°C, 40 minutes
Fe 2 Ta 5Cr	2%	5%	Balanced	1370°C, 1 hour	700°C, 40 minutes
Fe 2 Ta 7Cr	2%	7%	Balanced	1370°C, 1 hour	700°C, 40 minutes

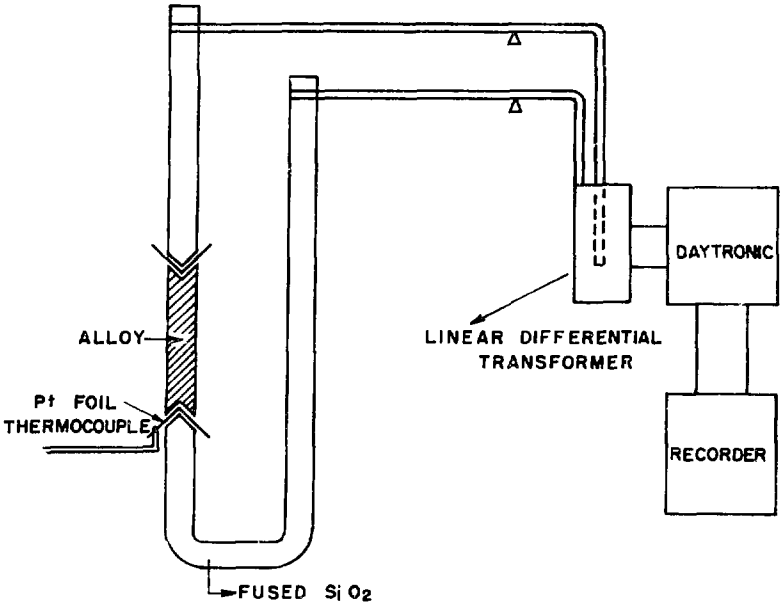
ALLOY
Pt FOIL
THERMOCOUPLE
FUSED Si O2
LINEAR DIFFERENTIAL
TRANSFORMER
DAYTRONIC
RECORDER
XBL 7112 - 7691

Fig. 4

TABLE II. PHASE TRANSFORMATION TEMPERATURES
DETERMINED BY DILATOMOMETRY AND METALLOGRAPHY

		$\alpha \rightarrow \gamma$		$\gamma \rightarrow \delta$		$\gamma + \delta \rightarrow \delta$ $Fe_2Ta + \delta \rightarrow \delta$
		D	M	D	M	M
	3 Cr	880-900°C		1230°C∿	∿1210°C	∿1300°C
1 Ta	5 Cr	870-890°C	890-905°C	1210°C∿	∿1200°C	∿1280°C
	7 Cr	860-880°C		1160°C∿	∿1180°C	∿1250°C
	3 Cr	880-900°C		1200°C∿	1200°C∿	1340°C∿
2 Ta	5 Cr	860-880°C		1200°C∿	1200°C∿	1360°C∿
	7 Cr	860-870°C		1160°C∿	∿1180°C	1370°C∿
Binary		974°C		1238°C		1340°C

D: Dilatometer work

M: Metallographic work

XBB 7112-5985

Fig. 5

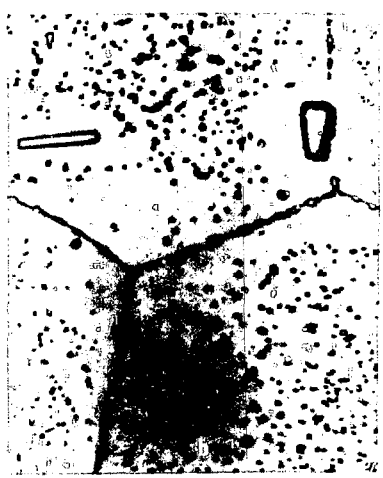

XBB 7112-5969

Fig. 6

XBB 7112-5983

Fig. 7

XBB 7112-5984

Fig. 8

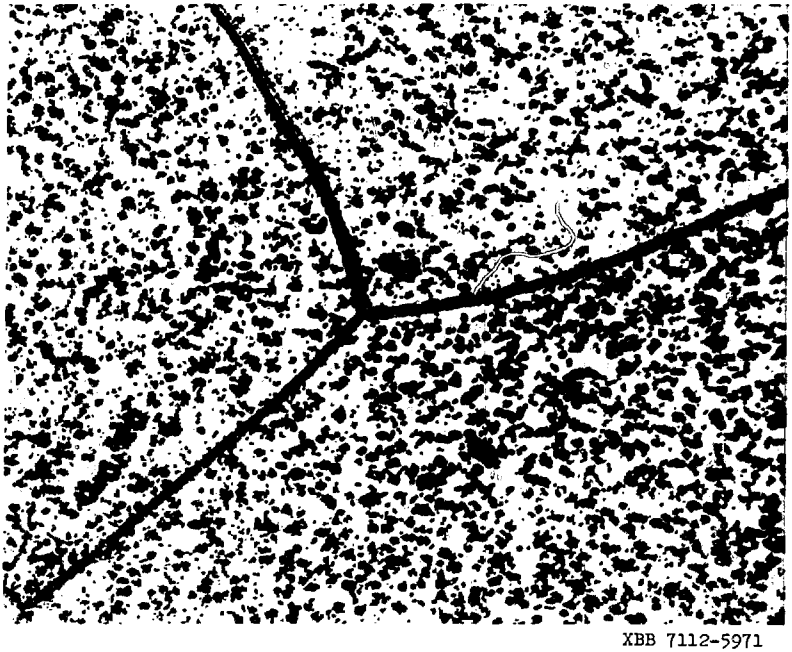

XBB 7112-5971

Fig. 9

determination by the metallographic method were held at 860°C for 12 hours, and then heated up to 890°C and 905°C respectively, at a heating rate of 1°C/minute, followed by quenching into salt water. (Fig. 10.)

Tensile specimens were quenched from 1320°C after 1 hour solution treatment into 45°C water. Three 1 a/o Ta alloys had no cracks while three 2 a/o Ta alloys had large transgranular cracks after this hot water quench.

Aging of solution treated specimens was performed in a molten salt bath at 700°C for 45 minutes. After aging, these specimens were air cooled.

Spheroidization treatment was carried out in protective steel bags.

D. Hardness Tests

Micro Vickers hardness tests were made by Seitz' Miniload Hardness Tester with the load of 2 Kg. For each hardness measurement, at least six indentations were made.

E. Tensile Tests

The mechanical properties of heat treated alloys were determined for flat specimens (1" gage length, 1/8" width and 1/10" thickness) and round specimens (1" gage length and 1/4" nominal diameter). An Instron tensile testing machine was used at a strain rate of 4×10^{-3}/minute. The 0.2% offset yield strength and the ultimate tensile strength were determined from the chart record, and the elongation was measured with a microscope. The fracture surface was examined by the Scanning Electron Microscope at 25 KV.

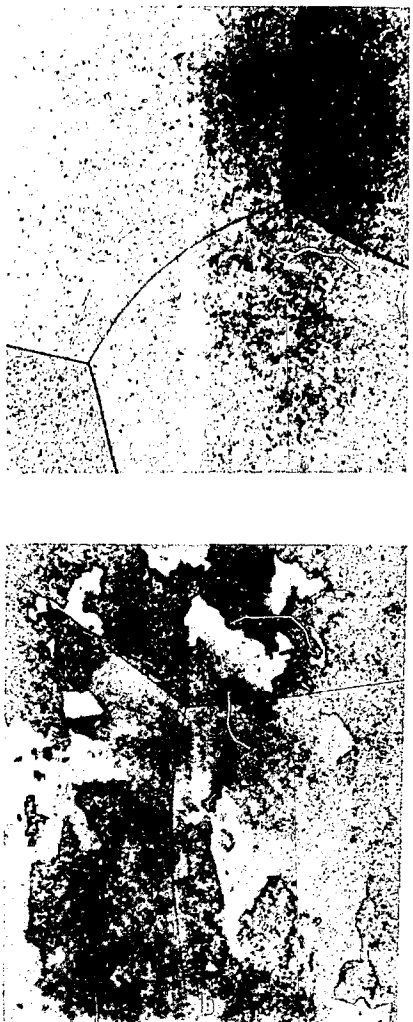

XBB 7112-5972

Fig. 10

F. X-ray Analysis of the Second Phase Particles

A Fe-1Ta-7Cr alloy specimen from the hot rolled rod was heated at 1100°C for 5 hours to get spherical particles of about two micron size. These particles were extracted by solution using H_2O_2 25 parts, H_2O 15 parts and HF 2 parts.

X-ray powder diffraction patterns of these extracted particles were obtained at 50 KV by Debye Scherra Camera and with a chromium target. The exposure time was 21 hours. A correction was made for film shrinkage. The X-ray diffraction results are shown in Table III.

G. Optical Microscopy

Specimens were ground on emergy papers and polished with 1.0 micron diamond paste and finally polished with 0.5 micron Al_2O_3 powder.

For the low chromium alloys, 5% Nital etching solution was used and for the higher chromium alloys, Kalling's reagent was employed.

H. Scanning Electron Microscopy

JSM-U3 Scanning Electron Microscope was utilized to study the grain boundary and matrix precipitation morphology. Specimens were polished and overetched. The surface was tilted 30 degrees toward the incident beam. The fracture surface after the tensile test was also examined.

TABLE III. X-RAY POWDER DIFFRACTION PATTERN OF THE SECOND PHASE

Line number	d (Å)	I/I_1
1	4.141	30
2	3.905	30
3	3.665	30
4	2.843	30
5	2.401	80
6	2.207	100
7	2.074	20
8	2.042	90
9	2.009	60
10	1.465	40
11	1.386	50
12	1.346	100
13	1.307	70

III. RESULTS AND DISCUSSIONS

A. Phase Relations in the Fe-Ta-Cr Ternary System

The equilibrium phase diagrams of Fe-Ta system,[3] Fe-Cr system[4] and Cr-Ta system[5] are shown in Figs. 1, 2, and 3. However, little work has been done for the Fe-Ta-Cr ternary system and the phase relationships are not very well known.

Dilatometer analysis (Table II) showed that the γ-δ phase transformation temperature had been lowered about 60°C and the α-γ phase transformation temperature had been lowered about 100°C by the addition of 7 atomic percent of chromium to Fe-Ta binary alloys. The results of the metallographic examination agreed reasonably with the dilatometer analysis.

The binary phase diagrams indicate that there are two possible Laves phases, Fe_2Ta which is a $MgZn_2$ type hexagonal Laves phase, and Cr_2Ta which is a $MgCu_2$ type cubic Laves phase. The two kinds of Laves phases will compete to form in the ternary alloys.

According to thermodynamic data, the heat of formation of Fe_2Ta phase[6] and Cr_2Ta phase[7] are as follows:

ΔH_f, Fe_2Ta = -6,077 cal/g-atom

ΔH_f, Cr_2Ta = -2,047 cal/g-atom

Thus the formation of Fe_2Ta is much more preferable to that of Cr_2Ta from the ΔH values of the two. The high Fe:Cr ratio also favors the formation of the Fe_2Ta over Cr_2Ta.

According to Kehsin Kuo's paper,[8] the formation of complex Laves phase like $(Fe,Cr)_2Ta$ etc. will not happen. Laves phase of AB_2 could be replaced by $A(C,D)_2$ where C is located to the left of B in the periodic

table and D to the right of B. That is, Fe_2Ta could be replaced by $(Cr,Ni)_2Ta$ or $(Cr,Co)_2Ta$ but not by $(Fe,Cr)_2Ta$. Therefore, the conclusion is that Fe_2Ta is the only stable Laves phase in this ternary system. The X-ray diffraction pattern (Table III) of the second phase particles agreed closely with the ASTM powder diffraction pattern file of Fe_7Ta_3 phase. The X-ray diffraction pattern in Fe-Ta binary system[2] was also that of Fe_7Ta_3. The stoichiometric compositions not being Fe_2Ta in binary and ternary alloys might be due to the possible solubility range of Laves phase according to Leo Brewer's theory.[9]

Results of the dilatometer work and the metallographic work (Table II) show that for a Fe-1Ta-5Cr alloy, the δ phase decomposes eutectoidally during cooling at 1200°C,

$$\delta \text{ (BCC)} = \gamma \text{ (FCC)} + Fe_2Ta$$

and α phase decomposes peritectoidally during heating at 900°C,

$$\alpha \text{ (BCC)} = \gamma \text{ (FCC)} + Fe_2Ta$$

The iron rich portion of the Fe-Cr binary system indicates that chromium up to 7 atomic percent has the effect of lowering both the α-γ and γ-δ transformation temperatures. This was proved by dilatometry and metallographic work. When ordinary ferrite stabilizing elements are added to iron, they close the γ loop, decreasing the stability region of γ iron, expanding the ferrite region and raising the α-γ transformation temperature. The γ loop formed by chromium has an unusual shape up to 7 percent chromium and the γ region is extended to lower temperature. Further increase in chromium content will lower the γ-δ transformation temperature but will raise the α-γ transformation temperature.

Figure 5 shows the retained δ structure obtained by iced salt water quenching from the δ phase field. However, it was found that even on fastest quench into iced brine from the temperature range where γ was stable, γ iron always transformed into massive α iron (Fig. 6a and Fig. 7). Even during air cooling from the δ range, BCC iron was retained and did not transform into γ. (Fig. 9). Thus the alloy of hypoeutectoid composition quenched from (δ+γ) region shows microstructure like Fig. 6a, while the hypereutectoid composition in δ+Fe_2Ta region has the microstructure of Fig. 6b.

Experimental results show that for hypoeutectoid alloys (Fe-1Ta-3Cr, and Fe-1Ta-5Cr), the temperature range of the solid solutions, δ and δ+γ, is lowered with increasing chromium content. For hypereutectoid alloys (Fe-1TA-7Cr, Fe-2Ta-3Cr, Fe-2Ta-5Cr and Fe-2Ta-7Cr), the δ-Laves phase solubility line is shifted to the lower concentrations of Ta. The eutectoid composition was also shifted to lower tantalum concentrations. The effects of chromium on Fe-Ta binary phase diagram are summarized in Fig. 11.

B. Morphology and Kinetics of Laves Phase Precipitation

(1) Second Phase Identification

As mentioned above, it was found that Fe_2Ta was the only stable phase in the ternary system.

(2) Aging Characteristics

The age hardening characteristics of four ternary alloys are shown in Fig. 12. The peak hardness on aging at 700°C occurred at 40 minutes, which was quite similar to that of binary alloys.[2] This indicates that chromium does not affect the aging characteristics of Fe-Ta binary

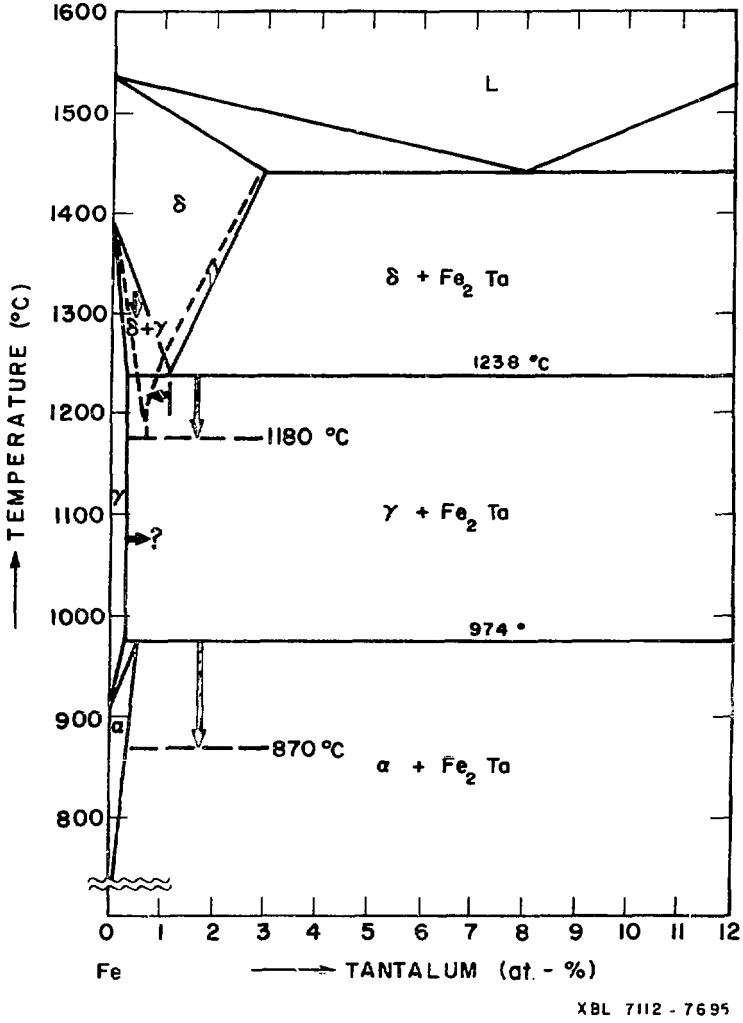
1600
1500
1400
1300
1200
1100
1000
900
800
TEMPERATURE (°C)
L
δ
δ + Fe2 Ta
δ+γ
1238 °C
1180 °C
γ
γ + Fe2 Ta
?
974 °
α
870 °C
α + Fe2 Ta
0 1 2 3 4 5 6 7 8 9 10 11 12
Fe
TANTALUM (at. - %)
XBL 7112 - 7695

Fig. 11

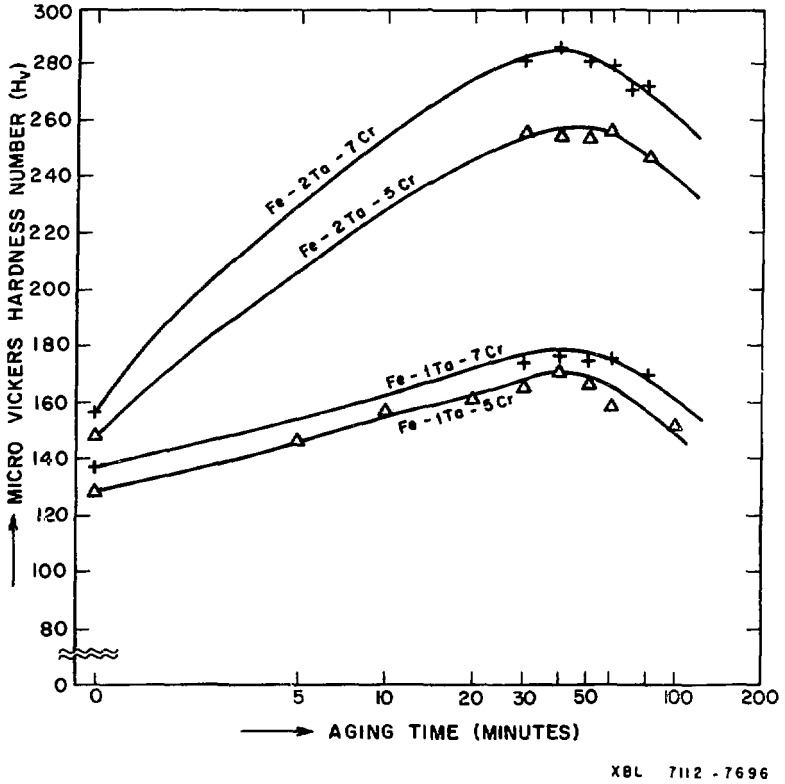
MICRO VICKERS HARDNESS NUMBER (H_V)
300
280
260
240
220
200
180
160
140
120
100
80
0
Fe - 2Ta - 7Cr
Fe - 2Ta - 5Cr
Fe - 1Ta - 7Cr
Fe - 1Ta - 5Cr
0
5
10
20
30
50
100
200
AGING TIME (MINUTES)
XBL 7112 - 7696

Fig. 12

system. The only difference was the small increase in hardness, which could be attributed to the solid solution hardening effect by chromium.[10]

R. H. Jones[2] found that the precipitation process in Fe-Ta binary alloy was continuous, with heterogeneous nucleation occurring. The nucleation sequence was grain boundaries, dislocations, and matrix. The precipitates were rather plate shaped and not spherical. Figure 13 shows the microstructure of binary alloy aged to its peak hardness at 700°C. The grain boundary precipitation was nearly continuous which was responsible for the brittle character of the aged binary alloys.

In the ternary alloys, however, particles were plate and spherical shaped, as shown in Fig. 14. Some grain boundaries in the aged alloys showed discontinuous films. (Fig. 15). The chromium seemed to have changed the surface energy, thus causing some spheroidization of grain boundary and matrix particles during the aging treatment.

C. Spheroidization of Grain Boundary and Matrix Precipitates

Spheroidization in the binary alloy was accomplished by cycling through the α-γ allotrophic phase transformation.[2]

In the ternary alloys, some grain boundary films were already broken up and some particles were rather spherical before the spheroidization treatment. However, the degree of spheroidization was not sufficient to eliminate the brittleness of the lower chromium alloys; thus, it was necessary to use the α-γ transformation treatment for these materials.

Spheroidization treatment at 1100°C for 5 minutes, 10 minutes, 30 minutes and 60 minutes, were used, and at 950°C for 10 minutes, 25 minutes, 1 hour, 5 hours, and 10 hours. Multicycling treatments

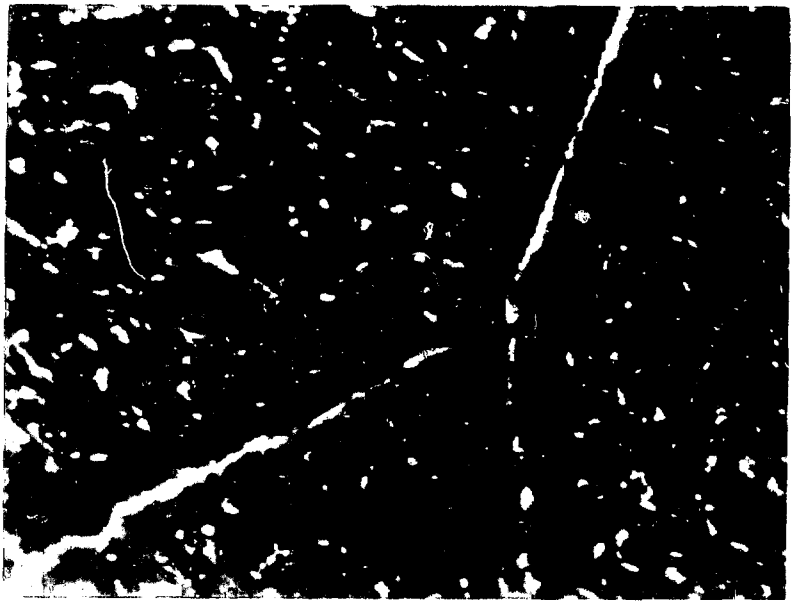

XBB 7112-5977

Fig. 13

XBB 7112-5975

Fig. 14

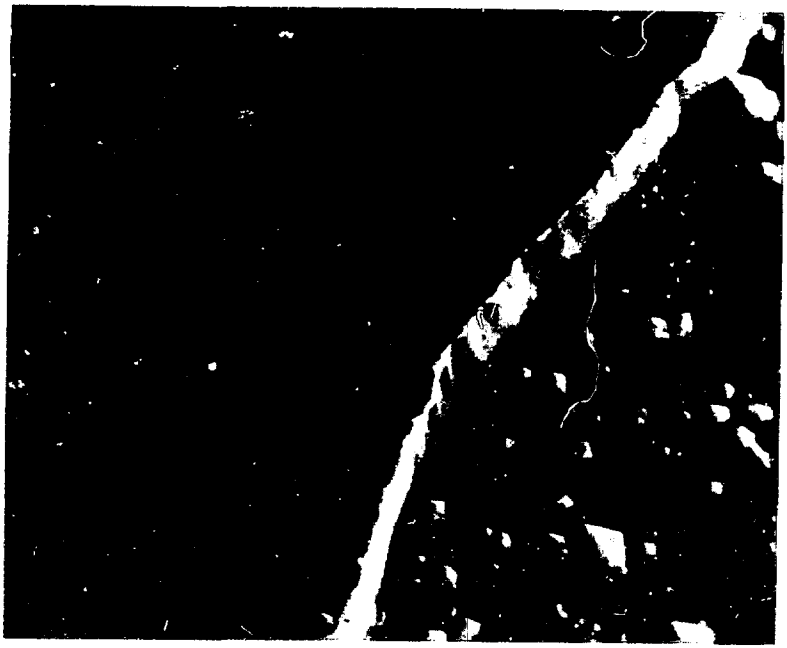

XBB 7112-5980

Fig. 15

consisting of 1 cycle, 2 cycles, 5 cycles and 10 cycles were also used. (The total duration of spheroidization time in $\gamma+Fe_2Ta$ region was 2 hours for all multicycling treatments.) Figures 16 through 20 show the scanning electron microscope pictures of the spheroidized structures.

For the binary alloys, it took 10 minutes to break up the continuous boundaries at 1100°C, but in the ternary alloys, an equivalent spheroidization occurred in less than 10 minutes. In the later, much shorter time could be used to obtain enough spheroidization at 1100°C and 950°C.

D. Mechanical Properties

(1) Effect of Spheroidization Temperature on Mechanical Properties

Figures 21, 22, and 23 show how the spheroidization temperature in the $\gamma+Fe_2Ta$ region affects the hardness of Fe-1Ta-5Cr alloy. In Figure 21, the linear dependence of hardness on temperature can be seen. Thus the mechanical properties for any spheroidization temperature within the $\gamma+Fe_2Ta$ range (900°C-1200°C) can be calculated as follows:

$$Hv = 146 + 0.315 \times (Ts-900°C)$$

where Hv is the Micro Vickers hardness number and Ts is the spheroidizing temperature in °C.

The peak aged Micro Vickers hardness for Fe-1Ta-5Cr alloy after aging was 109; the spheroidization treatments above 975°C produced an added increment of hardness.

(2) Effect of Spheroidization Time on Mechanical Properties

The Micro Vickers hardness and other mechanical properties for different spheroidization time are shown in Figs. 22 and 23. The spheroidization time did not affect the mechanical properties much, even though the particles coarsened during spheroidization.

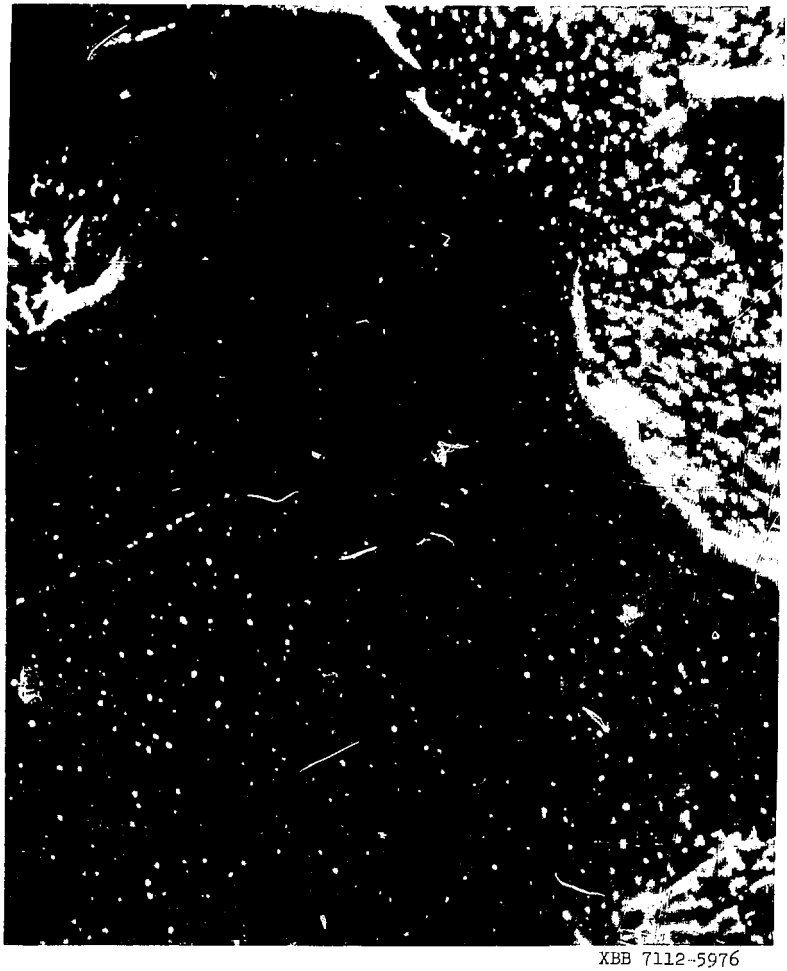

XBB 7112-5976

Fig. 16

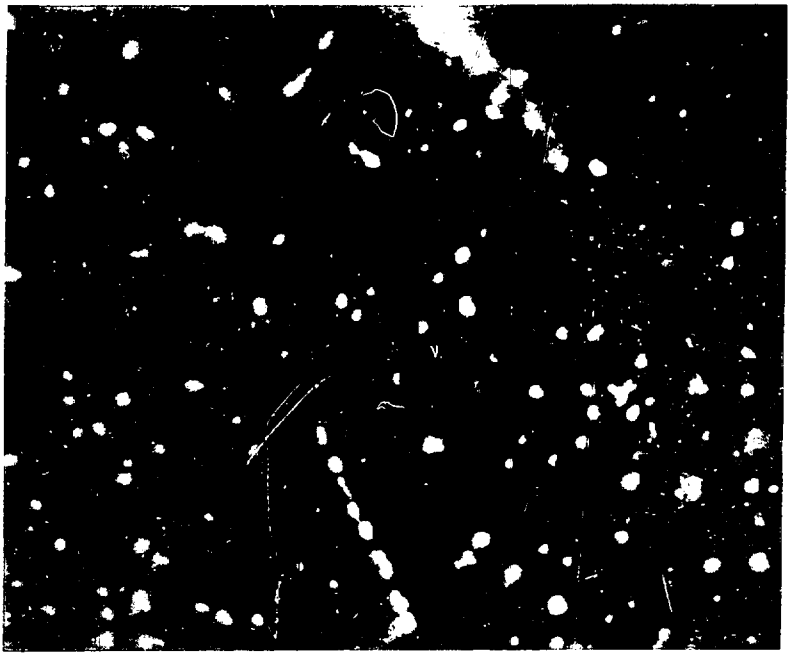

XBB 7112-5981

Fig. 17

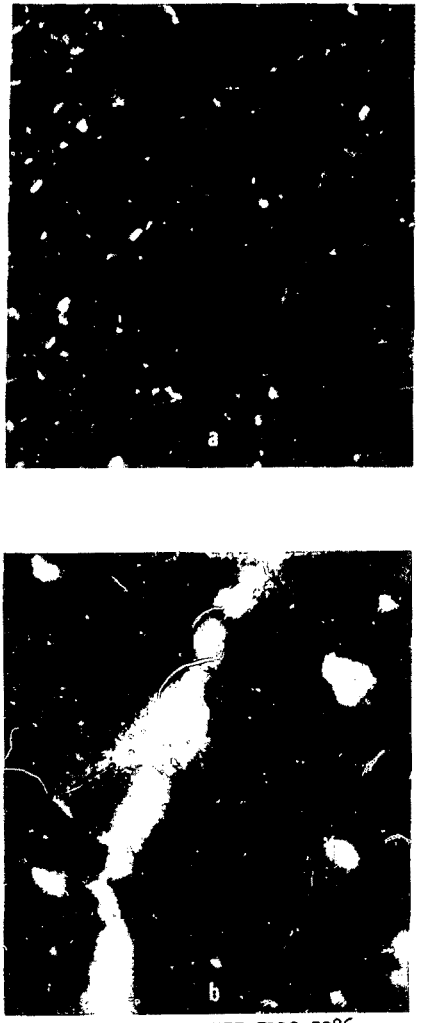

XBB 7112-5986

Fig. 18

XBB 7112-5974

Fig. 19

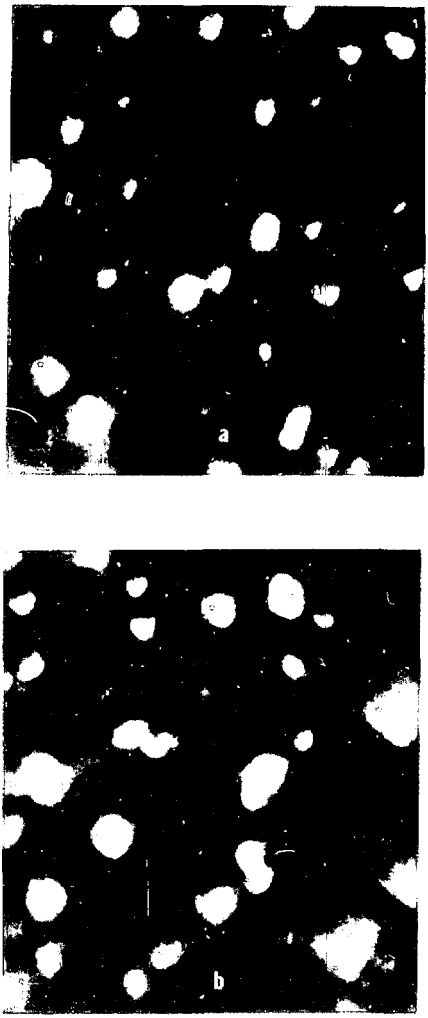

XBB 7112-5970

Fig. 20

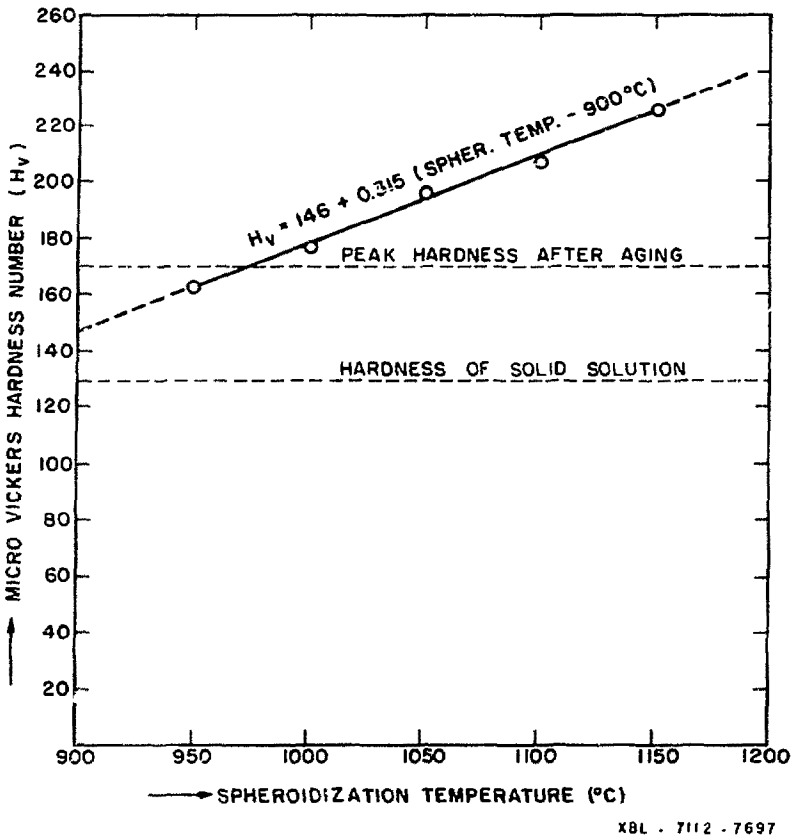
260
240
220
200
180
160
140
120
100
80
60
40
20
MICRO VICKERS HARDNESS NUMBER (H_V)
H_V = 146 + 0.315 (SPHER. TEMP. - 900°C)
PEAK HARDNESS AFTER AGING
HARDNESS OF SOLID SOLUTION
900
950
1000
1050
1100
1150
1200
SPHEROIDIZATION TEMPERATURE (°C)
XBL . 7112 . 7697

Fig. 21

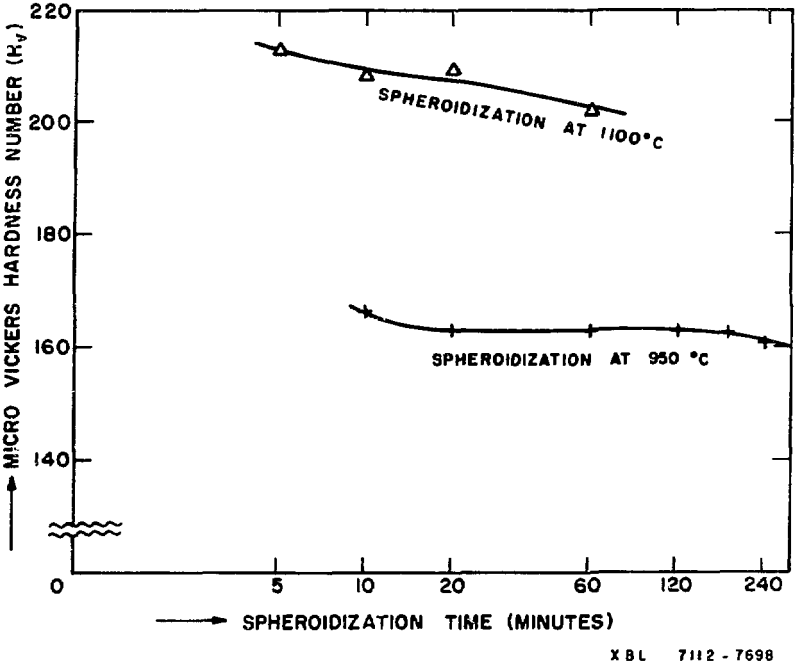
220
200
180
160
140
0
MICRO VICKERS HARDNESS NUMBER (H_v)
SPHEROIDIZATION AT 1100°C
SPHEROIDIZATION AT 950 °C
5
10
20
60
120
240
SPHEROIDIZATION TIME (MINUTES)
XBL 7112-7698

Fig. 22

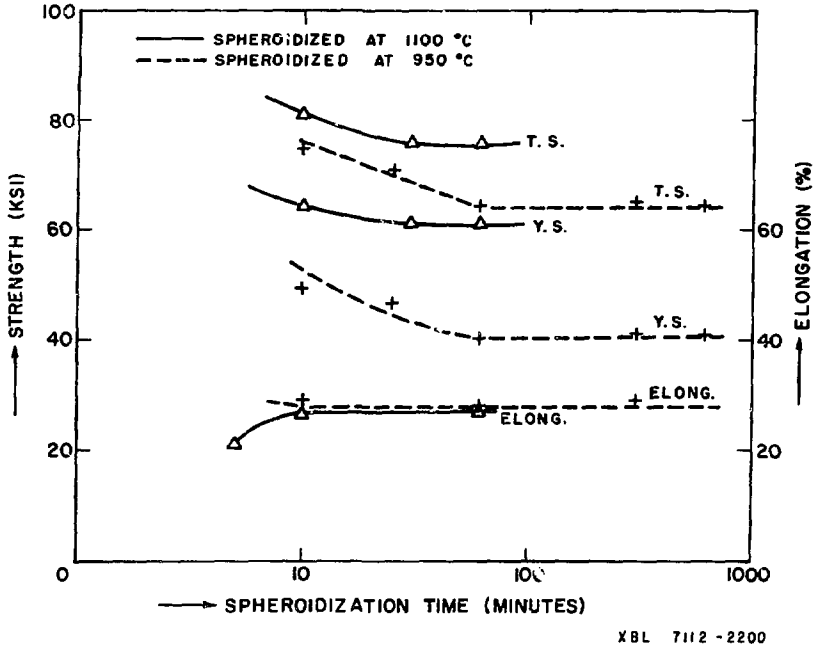
SPHEROIDIZED AT 1100 °C
SPHEROIDIZED AT 950 °C
T. S.
T. S.
Y. S.
Y. S.
ELONG.
ELONG.
STRENGTH (KSI)
ELONGATION (%)
100
80
60
40
20
0
60
40
20
10
1000
SPHEROIDIZATION TIME (MINUTES)
XBL 7112-2200

Fig. 23

(3) Effect of Cooling Rate on Mechanical Properties

Different cooling rates gave different hardness and these are shown in Fig. 24. Cooling rate affects the microstructure and substructure, and hence might be expected to produce the observed results.

(4) Effect of Chromium Content on Mechanical Properties

The effect of chromium content on the mechanical properties of aged specimens is shown in Fig. 25 and that of spheroidized specimens is shown in Fig. 26. A significant difference can be seen between the binary and ternary alloys. For the aged condition, the binary alloy showed almost zero elongation while the ternary alloys had elongation values up to 25% (for 7 a/o chromium alloy). The ductility increased with chromium content. The partly spheroidized grain boundary precipitates after aging were responsible for the higher ductility.

For the spheroidized specimens, the strength increased with increasing chromium content and the ductility decreased with increasing chromium content, as can be seen in Fig. 26.

(5) Effect of Multicycling

After multicycling at 950°C (5 cycles, each cycle 30 minutes holding at 950°C and cooling to room temperature), the strength was a little bit lower than that of the single cycled specimen. However, the elongation was much larger (33% elongation). An interesting effect of multicycling was that it altered the grain size markedly. Figures 27, 28a, and 28b show the grain sizes of aged, spheroidized (single cycled) and multicycled specimen of Fe-1Ta-5Cr alloy respectively. Figure 20a shows the particle shape in a single cycled specimen and Fig. 20b shows that in a multicycled specimen.

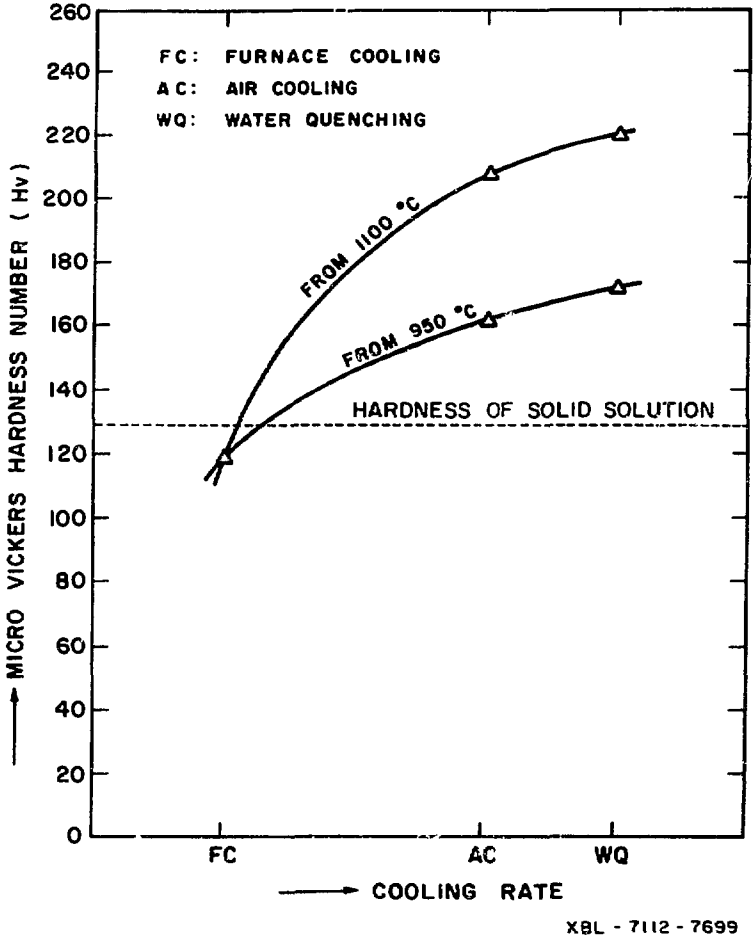
FC: FURNACE COOLING
AC: AIR COOLING
WQ: WATER QUENCHING
FROM 1100 °C
FROM 950 °C
HARDNESS OF SOLID SOLUTION
MICRO VICKERS HARDNESS NUMBER (Hv)
260
240
220
200
180
160
140
120
100
80
60
40
20
0
FC
AC
WQ
COOLING RATE
XBL - 7112 - 7699

Fig. 24

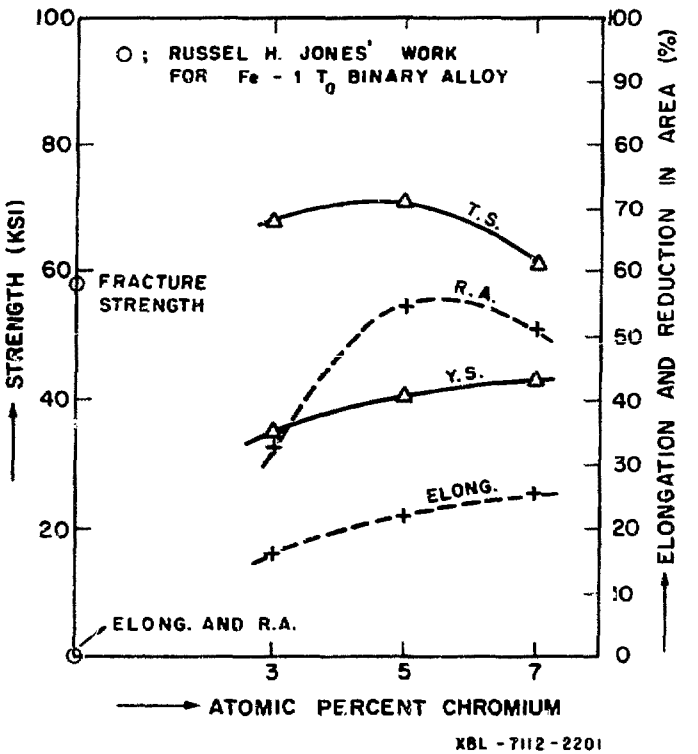
O ; RUSSEL H. JONES' WORK
FOR Fe - 1 T_0 BINARY ALLOY
T.S.
R.A.
Y.S.
ELONG.
FRACTURE STRENGTH
ELONG. AND R.A.
STRENGTH (KSI)
ELONGATION AND REDUCTION IN AREA (%)
ATOMIC PERCENT CHROMIUM
100
80
60
40
20
0
90
70
30
10
3
5
7
XBL-7112-2201

Fig. 25

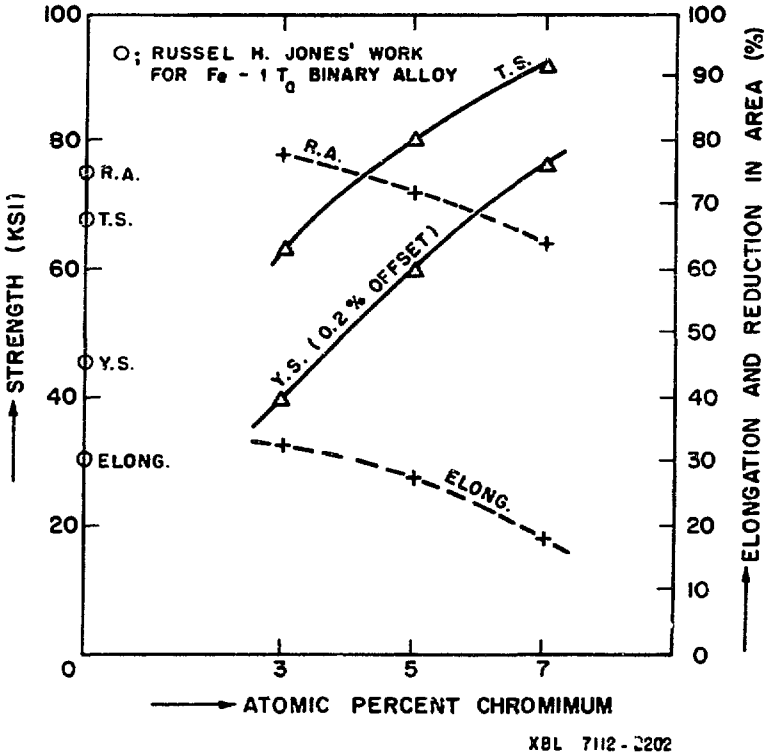
O; RUSSEL H. JONES' WORK
FOR Fe - 1 T_Q BINARY ALLOY
T.S.
R.A.
Y.S. (0.2 % OFFSET)
ELONG.
R.A.
T.S.
Y.S.
ELONG.
STRENGTH (KSI)
ELONGATION AND REDUCTION IN AREA (%)
ATOMIC PERCENT CHROMIMUM
0
3
5
7
20
40
60
80
100
10
30
50
70
90
XBL 7112-3202

Fig. 26

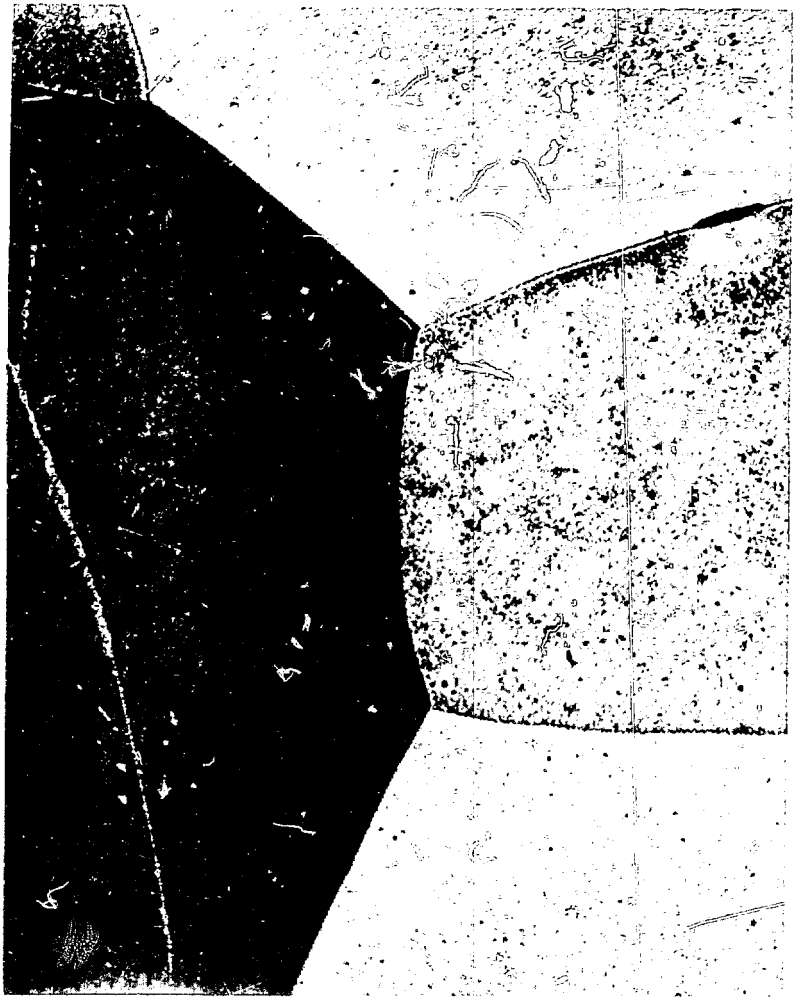

XBB 7112-5982

Fig. 27

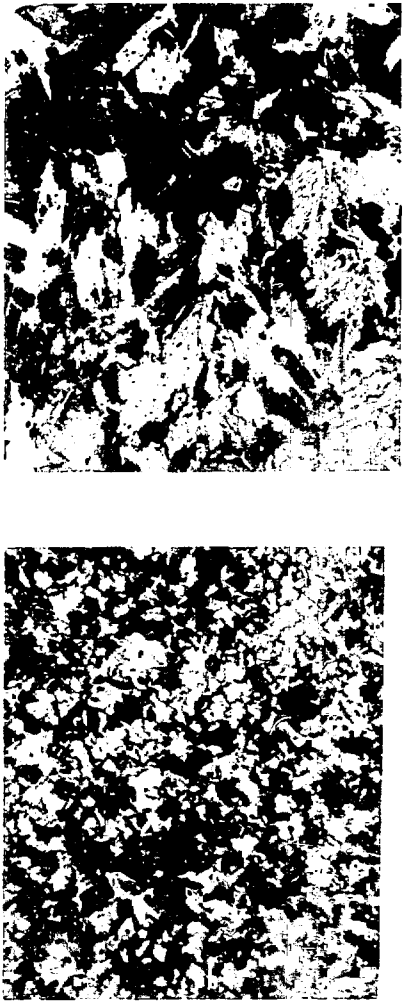

XBB 7112-5973

Fig. 28

(6) Effect of Chromium Content on the Oxidation Resistance

Spheroidization treatments without protective steel bags at 1100°C for 10 minutes showed that for 3Cr and 5Cr alloys, oxide and scales were observed on the surface of the specimens but for 7Cr alloys, no scales were observed after spheroidization treatments.

(7) Fracture Characteristics

For the aged specimen, the scanning electron microscope pictures of the fracture surface consisted of a combination of river and cup-and-cone patterns. (Fig. 29). This dual character seemed to be due to the partly broken grain boundary precipitates. The fracture surface of the binary alloys after aging was that of a completely brittle fracture, showing only the river pattern.

For the spheroidized specimen, the fracture characteristics was th[illegible] of completely ductile material, as shown in Fig. 30.

XBB 7112-5979

Fig. 29

XBB 7112-5978

Fig. 30

IV. CONCLUSIONS

(1) The α-γ phase transformation temperature was lowered about 100°C by adding 7 a/o chromium, and the γ-δ transformation temperature was lowered about 60°C, relative to the binary phase diagram.

(2) The eutectoid composition was shifted by the addition of Cr to the lower concentration of Ta.

(3) The second phase in the ternary system was established as the Laves phase, Fe_2Ta.

(4) The age hardening characteristics were similar to those of the binary alloys.

(5) The grain boundaries of the aged specimens of the ternary alloys were not completely continuous. Spheroidization in ternary alloys occurred in less than 10 minutes.

(6) The strength of the ternary alloy increased with increasing spheroidizing temperature. The spheroidization treatment could be used as the hardening treatment. In ternary alloys, almost the same strength could be obtained by 950°C spheroidization; this was 150° lower than the spheroidization temperature for binary alloys.

(7) The strength of the ternary alloys after spheroidization increased with chromium content and the ductility after spheroidization decreased with chromium content. For the aged specimens, the ductility increased with increasing chromium content.

(8) By multicycling, the ductility could be increased and a fine grain size could be obtained.

(9) The oxidation resistance of the ternary alloys increased with increasing chromium content.

ACKNOWLEDGMENTS

The author wishes to express his appreciation and deep gratitude to Professor Earl R. Parker and Professor Victor F. Zackay for their continued guidance and encouragement for this investigation.

Special thanks are due to Professor Richard M. Fulrath for his kind help in dilatometer work. Thanks are also due to Mr. George M. Gordon and Mr. George Georgakopoulos for their help in X-ray analysis and Scanning Electron Microscope work, to Mr. Russel H. Jones and Mr. Go Sasaki for their helpful suggestions and discussions.

The author also wishes to express his gratitude to Kelly Radmilovic for her help in typing, to Reida Officer for art work, to Phila Witherila and Doug Kreitz for their help in photography.

This work was performed under the auspices of the Unite States Atomic Energy Commission through the Inorganic Materials Research Div. of the Lawrence Berkeley Laboratory.

REFERENCES

1. G. Sasaki, Mechanical Properties of Laves Phases, Dec. 1970, Univ. of Calif., Berkeley, Lawrence Radiation Laboratory, UCRL-20301.

2. R. H. Jones, Ph.D. Thesis, Univ. of Calif., Berkeley, Lawrence Berkeley Laboratory, LBL-171, Oct 1971.

3. A. K. Sinha and W. Hume-Rothery, JISI, 1967, Vol. 205, p. 671.

4. M. Hansen and K. Anderko, Constitution of Binary Alloys, p. 527, McGraw-Hill, New York, 1958.

5. R. P. Elliot, Constitution of Binary Alloys, 1st Suppl. p. 362, McGraw-Hill, New York, 1965.

6. T. N. Rezukhina, W. N. Drobishew, L. I. Krawtshenko, B. Pokarew, The Thermodynamic Studies of Alloys of Refractory Metals by EMF Method with Solid Electrolytes at High Temperatures, Sept. 1969.

7. P. Feschotte and O. Kubaschewski, Thermodynamic Properties of the Laves Phase, Cr_2Ta, June 1964.

8. Kehsin Kuo, Ternary Laves and Sigma-Phases of Transition Metals, Acta Met., Vol. 1, Nov 1953, p. 720.

9. Lew Brewer, Prediction of High Temperature Metallic Phase Diagrams, UCRL-10701, 1965.

10. E. C. Bain and H. W. Paxton, Alloying Elements in Steels, 2nd Ed., ASM, 1966.

FIGURE CAPTIONS

Fig. 1. Equilibrium phase diagram: Fe-Ta system.

Fig. 2. Equilibrium phase diagram: Fe-Cr system.

Fig. 3. Equilibrium phase diagram: Cr-Ta system.

Fig. 4. Schematic diagram of the dilatometer analysis.

Fig. 5. Micrograph: Solid solution (δ region) of the Fe-1Ta-5Cr alloy, quenched from 1320°C, X200.

Fig. 6a. Micrograph: (δ + γ) region of the Fe-1Ta-5Cr alloy, quenched from 1260°C, X400.

Fig. 6b. Micrograph: (δ + Fe_2Ta) region of the Fe-1Ta-7Cr alloy, quenched from 1200°C, X400.

Fig. 7. Micrograph: (γ + Fe_2Ta) region of the Fe-2Ta-5Cr alloy, quenched from 1100°C, X400.

Fig. 8. Micrograph: (α + Fe_2Ta) region of the Fe-1Ta-5Cr alloy, furnace cooled from 950°C, X200.

Fig. 9. Micrograph: Air cooled from 1370°C, Fe-2Ta-5Cr alloy, X400.

Fig. 10a. Micrograph: Fe-1Ta-5Cr alloy, solution treated and quenched, held at 860°C for 12 hours and 890°C for 2 hours, X100.

Fig. 10b. Micrograph: Fe-1Ta-5Cr alloy, solution treated and quenched, held at 860°C for 12 hours and slowly heated up, held at 905°C for 2 hours, X100.

Fig. 11. The effect of 7% chromium on Fe-Ta binary phase diagram.

Fig. 12. Age hardening curves for four alloys.

Fig. 13. Scanning electron micrograph: Fe-1Ta binary alloy aged at 700°C for 60 minutes, X10,000.

Fig. 14. Scanning electron micrograph: Matrix precipitation of Fe-1Ta-7Cr alloy on aging, X10,000.

Fig. 15. Scanning electron micrograph: Grain boundary precipitation of Fe-1Ta-7Cr alloy on aging, X3,000.

Fig. 16. Scanning electron micrograph: Grain boundary and matrix particles of Fe-1Ta-5Cr alloy spheroidized at 1100°C for 10 minutes, X3,000.

Fig. 17. Scanning electron micrograph: Grain boundary and matrix particles of Fe-1Ta-5Cr alloy spheroidized at 1100°C for 10 minutes, X10,000.

Fig. 18a. Scanning electron micrograph: Grain boundary and matrix precipitates of Fe-1Ta-5Cr alloy spheroidized at 950°C for 4 minutes, X10,000.

Fig. 18b. Scanning electron micrograph: Grain boundary and matrix precipitates of Fe-1Ta-5Cr alloy spheroidized at 950°C for 4 minutes, X30,000.

Fig. 19. Scanning electron micrograph: Fe-1Ta-5Cr alloy spheroidized at 950°C for 25 minutes, X10,000.

Fig. 20a. Scanning electron micrograph: Particle morphology in Fe-1Ta-5Cr alloy spheroidized at 950°C for 10 hours, X30,000.

Fig. 20b. Scanning electron micrograph: Particle morphology in Fe-1Ta-5Cr alloy 5-cycled at 950°C (30 minutes X5), X30,000.

Fig. 21. Dependence of the hardness of the Fe-1Ta-5Cr alloy on the spheroidization temperature.

Fig. 22. Plot of Micro Vickers Hardness vs spheroidization time.

Fig. 23. Mechanical properties of Fe-1Ta-5Cr alloy after spheroidizing at 1100°C and 950°C plotted as strength vs spheroidization time, and percent elongation and reduction in area vs spheroidization time.

Fig. 24. Effect of cooling rate on the hardness of Fe-1Ta-5Cr alloy.

Fig. 25. Mechanical properties of the ternary alloys (1% Ta) as a function of chromium content. Aged at 700°C for 40 minutes (before spheroidization).

Fig. 26. Mechanical properties of the ternary alloys (1% Ta) as a function of chromium content. Aged at 700°C for 40 minutes and spheroidized at 1100°C for 10 minutes.

Fig. 27. Micrograph: Fe-1Ta-5Cr alloy, solution treated and aged at 700°C for 40 minutes, X200.

Fig. 28a. Micrograph: Fe-1Ta-5Cr alloy, solution treated, aged at 700°C for 40 minutes and spheroidized at 1100°C for 10 minutes, X200.

Fig. 28b. Micrograph: Fe-1Ta-5Cr alloy, solution treated, aged and multicycled at 1100°C (30 minutes X5), X200.

Fig. 29. Scanning electron micrograph: Fracture surface of the aged Fe-1Ta-7Cr alloy, X300.

Fig. 30. Scanning electron micrograph: Fracture surface of the aged and spheroidized Fe-1Ta-5Cr alloy, X300.